Age-Associated Changes in the Retinal Nerve Fiber Layer and Optic Nerve Head

Nimesh B. Patel,[1] Mimi Lim,[2] Avni Gajjar,[1] Kelsey B. Evans,[1] and Ronald S. Harwerth[1]

[1]University of Houston College of Optometry, Department of Vision Sciences, Houston, Texas, United States
[2]State University of New York College of Optometry, New York, New York, United States

Correspondence: Nimesh B. Patel, University of Houston College of Optometry, Department of Vision Sciences, 505 J. Davis Armistead Building, Houston, TX 77204, USA; npatel@optometry.uh.edu.

Submitted: March 4, 2014
Accepted: July 10, 2014

Citation: Patel NB, Lim M, Gajjar A, Evans KB, Harwerth RS. Age-associated changes in the retinal nerve fiber layer and optic nerve head. *Invest Ophthalmol Vis Sci*. 2014;55:5134–5143. DOI:10.1167/iovs.14-14303

Purpose. Optical coherence tomography (OCT) measures of the retinal nerve fiber layer (RNFL) thickness and neuroretinal rim (NRR) parameters are often used as a surrogate for retinal ganglion cell content. The purpose of this study was to investigate the relationship between these morphological measures and the aging effects on these structures.

Methods. One hundred thirteen healthy individuals, aged 19 to 76 years, with no prior history of retinal of optic nerve head pathology were recruited. A circumpapillary and radial OCT scan centered on the optic nerve head (ONH) was used for data analysis. Transverse scaling was calculated for each subject using measures from optical biometry. Custom algorithms were used for morphological analysis of the ONH NRR and RNFL that included quantification of major retinal vascular contribution.

Results. There was a significant age-related loss of RNFL thickness (−0.23 μm/y, $R^2 = 0.24$, $P < 0.01$), major retinal vascular contribution (−0.03 μm/y, $R^2 = 0.07$, $P = 0.01$, neural rim volume (NRV, −0.004 mm³/y, $R^2 = 0.15$, $P < 0.01$), and minimum rim width (MRW, −1.77 μm/y, $R^2 = 0.23$, $P < 0.01$) before, and after, incorporating the Bruch's membrane opening size (sMRW, −1.86 μm/y, $R^2 = 0.22$, $P < 0.01$). When normalized, the rates of change for ONH NRR parameters (NRV, 0.69%/y and sMRW, 0.50%/y) exceeded that of RNFL thickness (0.19%/y, $P < 0.01$).

Conclusions. Although both RNFL and ONH NRR parameters contain axons of retinal ganglion cells, there are differences in age-related changes in these measures that should be considered in clinical application.

Keywords: aging, RNFL, neuroretinal rim, vasculature

The glaucomas are a group of optic neuropathies that are characterized by losses of retinal ganglion cells (RGCs) and associated thinning of the retinal nerve fiber layer (RNFL), cupping of the optic nerve head (ONH), and decrease in visual sensitivity.[1–4] In early stages of the disease, when visual fields may still be clinically normal, a critical assessment of the ONH and RNFL provide valuable information for initial diagnosis and management.[5,6] These structures are often assessed during an ophthalmoscopic evaluation, but the procedure has high inter- and intrasubject variability.[7–9] In contrast, objective in vivo imaging using optical coherence tomography (OCT) provides higher resolution and more repeatable measures.[10–14]

The standard OCT scan protocol used to assess the health of the optic nerve is a circumpapillary 12° diameter circular scan centered on the ONH. Global and localized RNFL thickness measures from this strategy have been shown to be reasonably sensitive for detection and progression of glaucomatous neuropathy.[15] Of recent, improved methods of using OCT volume or radial scans for assessing glaucoma associated changes in ONH morphology have been proposed. These measurements include the neuroretinal rim (NRR) area (RA), the minimum NRR width (MRW), and the NRR volume (NRV), all referenced to Bruch's membrane opening (BMO).[16–18] Each of these metrics, RNFL thickness, RA, MRW, and NRV, are considered to reflect the RGC axonal content of the retina.

Although morphological measures with OCT technology are repeatable, there are several aspects of the scan acquisition and analysis that are important to consider. Scans that are well centered and captured through a dilated pupil and have high image quality are needed for accurate analysis.[19–22] In addition, the location of the scan path is dependent on the optics of the imaging device and eye. Hence, in myopic eyes or eyes with a longer axial length, the RNFL scan path is further from the ONH rim margin where the nerve fiber layer is also thinner.[23–25] Incorporating transverse scaling in RNFL measures has been shown to improve the precision of these measures.[26–28] Similarly, it is logical that scaling principles should also be applied for analysis of ONH morphology.[24]

For the detection of optic neuropathies, it is important to differentiate pathological losses from normal age-related losses. Several histological studies that have evaluated RGC axons of the optic nerve or RGC cells in the retina have shown steady losses of cells with age.[29–33] Similarly, a majority of studies of OCT measurements have determined that the circumpapillary RNFL thickness becomes systematically thinner with age, but the age-related effects of OCT-derived ONH neural measures and their relationship to RNFL thickness have not been clearly delineated.[34–40] These measures also include both neuronal and nonneuronal components,[28,36,41] including glial and vascular tissue, that could exhibit age-related changes. In addition, ONH neural measures are dependent on the orientation of the axonal

bundles as they bend at the BMO, and it is possible that this orientation changes with the lamina structure in the aging eye (Bhakta AS, et al. *IOVS* 2014;55: ARVO E-Abstract 897).[42,43]

The present study was undertaken to investigate the relationship between OCT-derived morphological measures of the RNFL, MRW, and NRV and the aging effects on these structures.

Methods

Subjects

One hundred thirteen subjects with no history of ocular pathology were recruited from the University of Houston University Eye Institute clinics for this study. The study adhered to the tenets of the Declaration of Helsinki, and all aspects were reviewed by the Committee for Protection of Human Subjects at the University of Houston. Prior to collection of data, informed consent was obtained from all subjects.

Subjects were screened using a brief medical history, visual acuity assessment, 24-2 SITA standard visual fields, intraocular pressure measures, slit lamp examination, and a dilated fundus examination to ensure good ocular health. Only subjects with at least 20/30 best corrected acuity and no visual field defects or history of retinal pathology, optic nerve pathology, or ocular surgery were included. Subjects with a history of hypertension and/or diabetes were included only if there was no present or prior associated retinal or optic nerve pathology. One eye of each subject was randomly selected for data collection.

Optical Coherence Tomography

Data were acquired with the Spectralis HRA+OCT (Heidelberg Engineering, Heidelberg, Germany; software version 6.0), 30 minutes after the instillation of 1% tropicamide. Scans used for analysis included (1) a standard 12° circular scan, with Automatic Real Time (ART) averaging set at 40, and (2) a 12-line, 20° radial scan with an ART setting of 20. Prior to each scan capture, ART was engaged, and the scans were centered as best as possible on the ONH using anatomical structures visible on the infrared (IR-SLO) and B-scan images. Scans were repeated if image overlap was noted during averaging, or if any B-scan image quality fell below 25 dB. Image and scan acquisition data were exported in raw (.vol) files and coded so that the investigator was unaware of the subject's identity or age at the time of image analysis.

Ocular Biometry and Scaling

Ocular biometry including corneal curvature, anterior chamber depth, lens thickness, and axial length were measured using a noncontact optical biometer (Lenstar LS 900; Haag-Streit, Koeniz, Germany). For each subject, a customized three-surface schematic eye was constructed using principles described by Bennett and Rabbetts.[44–46] In brief, the eye in this model is considered an optical system with aligned spherical lenses and a spherical retinal surface. The cornea is a single and the first surface, that separates air ($n = 1$) from the aqueous ($n = 1.336$), while the lens represents the other two refractive surfaces. The crystalline lens curvature and refractive index were determined from normative data.[47,48] The distance from the second nodal plane, from this optical system, to the retina was used to calculate individualized transverse scaling. Additional details on this scaling methodology that incorporates both anterior segment optics and axial length are presented elsewhere.[27,28] Fixed retinal scaling was based on an emmetropic three-surface schematic eye, with a distance from the second nodal plane to the retina of 16.6 mm (transverse scaling = 289.2 μm/deg). No adjustments were made for axial scaling from those reported by the manufacturer because they are mainly dependent on the characteristics of the instrument imaging system.

RNFL Analysis

The standard circular B-scan and instrument determined segmentation of the RNFL were imported into MATLAB (The Mathworks, Natwick, MA, USA), and any errors in segmentation were manually corrected. When possible, vessels of the inner retina that made contact with the nerve fiber layer were included in the RNFL thickness. Prior to identification and marking of the major retinal vasculature, B-scans were scaled to a 1:1 aspect ratio using the calculated transverse scaling for that subject. Vasculature crossings along the circular scan path were marked on the IR-SLO image (Fig. 1A), and transferred to the OCT B-scan. Using these markings as a guide, the borders and center of each major vessel was marked and fit with a circle (Fig. 1C). This circular region was subtracted from the RNFL thickness to reduce the nonneuronal component and also used to calculate the vascular contribution. RNFL thickness was then converted to RNFL area by multiplying the average or global thickness by the calculated scan circumference (Equation 1). Finally, the RNFL area measures were transformed to a scaled thickness by dividing the calculated area by the nominal scan circumference for an emmetropic eye (Equation 2). Only global RNFL measures have been used for data analysis in the present study.

$$\text{Scan circumference}\,(\mu\text{m}) = 12^{\circ} \times \text{individualized transverse scaling}(\mu\text{m/deg}) \times \pi$$

$$\text{RNFL area} = \text{RNFL thickness} \times \text{Scan circumference} \quad (1)$$

$$\text{Nominal scan circumference}\,(\mu\text{m}) = 12 \times \text{nominal scaling} \times \pi$$

$$\text{Nominal scan circumference}\,(\mu\text{m}) = 12 \times 289.2\,\mu\text{m/deg} \times \pi = 10,901\ \mu\text{m}$$

$$\text{Scaled RNFL thickness} = \frac{\text{RNFL area}}{\text{Nominal scan circumference}} \quad (2)$$

ONH Analysis

Each ONH parameter (Fig. 1B) was calculated with both fixed (289.2 μm/deg) and custom transverse scaling. The dimensions of the ONH rim margin were determined by marking the RPE/BMO on each side of the ONH in 12 radial B-scans and fitting the resultant 24 points with an ellipse. The BMO was used because it is readily visible and thought to be a relatively stable reference for quantification of ONH parameters.[49] The inner limiting membrane (ILM) and basement membrane (BM) were manually delineated for each B-scan, and a spline fit was used for interpolating the BM within the region of the BMO. Two ONH NRR parameters, the minimum rim width (MRW) and neural rim volume (NRV), were calculated after scaling the scans to 1:1 μm. The MRW was determined as the shortest distance from the marked BMO opening and the ILM. Based on previous findings on the relationship between RA and disc size,[50,51] the MRW is expected to decrease with increase in disc area. Specifically, the RA is related to the MRW as RA ~ {(π

Investigative Ophthalmology & Visual Science

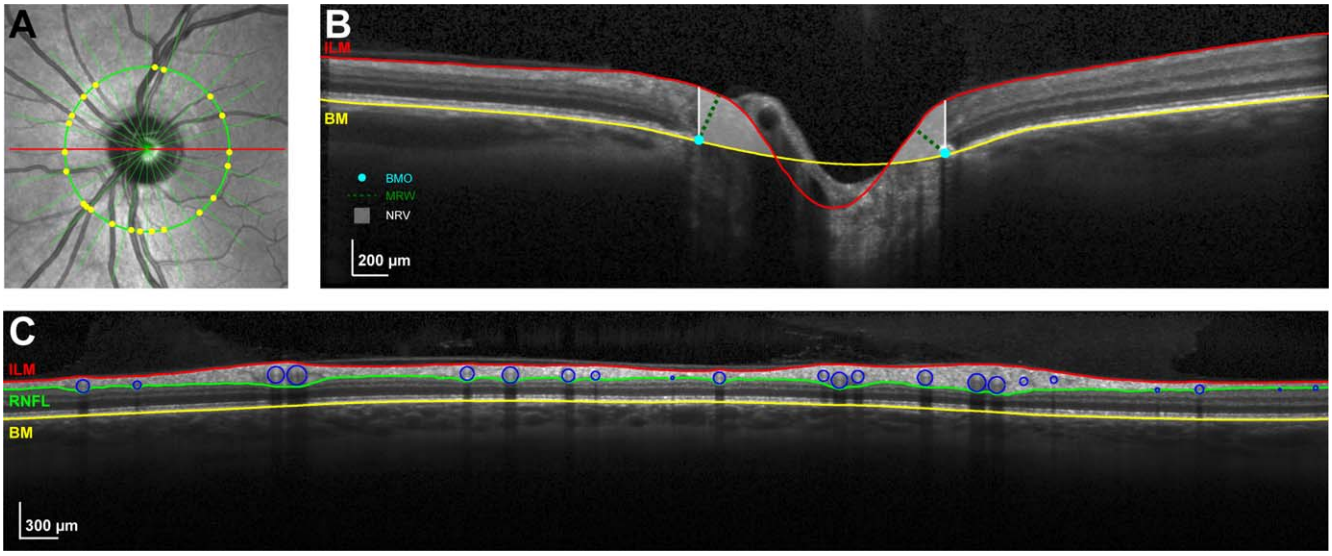

Figure 1. (**A**) IR-SLO image illustrating radial scans and the RNFL scan path used for ONH NRR and nerve fiber layer thickness analysis. All image analysis were done after scaling to 1:1 µm. (**B**) B-scan corresponding to the horizontal scan through the optic nerve (*red line* in [**A**]), with the ILM and BM segmentation. The BMO in each radial scan was manually marked (*blue dot*) and used as a reference to quantify the MRW (*green dashed line*) and NRV (*white shaded region*). (**C**) The segmentation of the RNFL was corrected to include the major retinal vasculature, which were then manually identified (*blue circles*) with the aid of the IR-SLO image (*yellow dots* in [**A**]). Thickness measures with and without major retinal vasculature were used for data analysis.

$\times$ BMO radius^2) $-$ [$\pi \times$ (BMO radius $-$ MRW)^2]}. To account for disc size, MRW was scaled (sMRW) using similar methods used to scale RNFL thickness. Specifically, the minimum rim area (MRA) was calculated by multiplying the BMO circumference and average MRW (Equation 3), and this measure was then converted to a scaled thickness (sMRW) by dividing it by the average scaled BMO circumference for subjects collected to date in our laboratory (4825 µm, Equation 4). In principal, the average BMO circumference, is expected to be different across ethnicities,[50,52] and can be replaced with any measure, resulting in similar scaled measures.

$$\text{BMO circumference}\,(\mu\text{m}) = \pi\left[3(a+b) - \sqrt{10ab + 3(a^2+b^2)}\right] \quad (3)$$

Where a and b are the major and minor axis of the best fit ellipse in micrometers.

$$\text{MRA}(\mu\text{m}^2) = \text{MRW} \times \text{BMO circumference}$$
$$\text{sMRW} = \frac{\text{MRA}}{4825\mu\text{m}} \quad (4)$$

To calculate the neural rim volume (NRV), a total retinal thickness map from the ILM and BM segmentation of the radial scans was first created, from three-dimensional representations of both surfaces. This thickness map was then scaled to 1 pixel/1 µm, and the tissue/pixel content above the splined BM plane within the three-dimensional BMO plane was used to compute the NRV.

All statistical analysis and plots reported were using either GraphPad Prism version 6.0 (GraphPad Software, La Jolla, CA, USA), Minitab 16 (Minitab, Inc., State College, PA, USA), or SigmaPlot 12.0 (Systat Software, San Jose, CA, USA).

Results

A total of 57 right and 56 left eyes of 113 subjects were analyzed for this study. All eyes were healthy as defined by the inclusion criteria. The mean age of subjects was 43.8 $\pm$ 17.5 years, with a range from 19 to 76 years of age, and neither sex nor ethnicity was considered in enrollment or analysis of the results of the study. Only the average/global measures of the RNFL and ONH parameters were included in the data analysis for the present study. All measures, other than age ($P < 0.01$) and fixed and custom scaled NRV ($P < 0.01$) were normally distributed as determined by the D'Agostino and Pearson normality test. The mean and median values for age, axial length, and scaled and fixed scaled measures are presented in the Table.

RNFL Thickness

The effects of individualized transverse scaling of OCT measurements and the nonneuronal vasculature contribution to the RNFL were studied using the group mean data. The mean RNFL thickness before scaling and vessel removal was 111.22 $\pm$ 9.4 µm, and there was a significant relationship between global RNFL thickness and axial length, with longer eyes having thinner measures (slope = $-$3.2 µm/mm, $R^2 = 0.23$, $P < 0.01$). After scaling to correct for differences in the subjects' ocular biometry, the mean RNFL area was 1.24 $\pm$ 0.09 mm^2, corresponding to a scaled thickness of 113.9 $\pm$ 8.4 µm, which was uncorrelated to axial length (slope = 0.74, $R^2 = 0.007$, $P = 0.19$). Overall, the major retinal vascular contribution to RNFL thickness was 15.6 $\pm$ 19 µm (13.8 $\pm$ 1.5%) for scaled global measures, but the vascular contribution to RNFL thickness varied with thickness. Specifically, eyes with greater scaled RNFL thickness had a larger vascular contribution in micrometers (slope = 0.1 µm/µm, $R^2 = 0.18$, $P < 0.01$), but this relationship was only marginally significant when the vascular contribution was expressed as a percentage (slope = $-$0.04 %/µm, $R^2 = 0.04$, $P = 0.05$). Thus, the results from the present study are consistent with previous investigations on separate groups of subjects that demonstrated that RNFL content does not vary with axial length and that the vasculature from the central retinal artery and vein make up a significant portion of RNFL thickness.[26,28,41,53]

Table. Mean and Median Measures for RNFL and NRR Parameters With Fixed and Custom Scaling

		Mean	SD	Median	Interquartile Range
	Age	43.77 y	17.58	41.52	25.44–61.49
	Axial length	24.63 mm	1.39	24.43	23.63–25.66
Fixed scaling	RNFL thickness	111.22 μm	9.41	110.45	103.92–119.29
	RNFL thickness MRV removed	95.98 μm	8.56	95.11	89.63–101.57
	NRV	0.42 mm^2	0.15	0.41	0.31–0.51
	MRW	323.41 μm	68.15	318.62	270.79–369.55
	sMRW	313.68 μm	65.23	299.65	262.62–355.13
	BMO	1.77 mm^2	0.36	1.76	1.49–2.05
Custom scaling	RNFL thickness	113.94 μm	8.40	113.60	107.84–119.49
	RNFL thickness MRV removed	98.29 μm	7.79	98.13	93.11–104.09
	NRV	0.45 mm^2	0.17	0.41	0.31–0.55
	MRW	320.15 μm	65.46	316.51	268.30–360.54
	sMRW	318.86 μm	69.19	308.70	265.98–361.29
	BMO	1.86 mm^2	0.40	1.83	1.58–2.09

ONH Parameters

The transverse magnification effects on the quantification of ONH parameters were investigated by comparing measurements with and without custom scaling. Using fixed transverse scaling, none of the ONH parameters (i.e., NRV, MRW, sMRW, or BMO area) was correlated with axial length ($P = 0.41$, $P = 0.18$, $P = 0.32$, and $P = 0.54$, respectively). However, when custom scaling was implemented, the measurements for BMO area (slope = 0.11 $mm^2/\mu m$, $R^2 = 0.15$), NRV (slope = 0.04 mm^3/mm, $R^2 = 0.11$), and sMRW (slope = 17.1 μm/mm, $R^2 = 0.12$) increased with axial length ($P < 0.01$), whereas MRW did not ($P = 0.08$). Further, with a multiple regression analysis to test whether NRV, BMO area, and axial length predicted MRW, the statistics indicated that BMO area and NRV together explained 91% of the variance ($F_{2,110} = 535$, $P < 0.01$). The MRW did not correlate significantly with BMO area (slope = –27.4 $\mu m/mm^2$, $R^2 = 0.02$, $P = 0.07$), but when the MRW was transformed to a scaled value (sMRW) using Equation 4, there was a significant inverse relationship with sMRW (slope = 60.5 $\mu m/mm^2$, $R^2 = 0.12$, $P < 0.01$). The relationship between the ONH NRR measures of scaled data for NRV and MRW/sMRW were more clearly defined by a power-function relationship, which is sensible because of the dimensions of the measures (volume versus linear). In addition, the ratio of probabilities (363.7) for Akaike information criteria (AICc) analysis supported the use of a simple power function ($y = ax^b$), compared to a linear fit. AICc analysis is a statistical method used to determine the simplest model for the best fit to the dataset.[54] Overall, the exponential relationship for sMRW as a function of NRV (Fig. 2B, $R^2 = 0.94$, $P < 0.01$) provided a better description of the relationship and accounted for a larger portion of the variance than for the MRW versus NRV relationship (Fig. 2A, $R^2 = 0.74$, $P < 0.01$).

The relationship between custom scaled ONH parameters and custom scaled RNFL thickness, after removal of major retinal vessels (RNFLV), showed that thickness was not significantly greater in eyes with a larger BMO area ($R^2 = 0.02$, p = 0.1). On the other hand, a significant relationship existed between scaled measures of RNFLV and NRV (Fig. 3A, slope = 0.01 $mm^3/\mu m$, $R^2 = 0.14$, $P < 0.01$), MRW (slope = 3.20 $\mu m/\mu m$, $R^2 = 0.14$, $P < 0.01$, data not shown), and sMRW (Fig. 3B, slope = 3.99 $\mu m/\mu m$, $R^2 = 0.20$, $P < 0.01$). It is important to note, however, that although there was significant variability, the relationships between RNFL and ONH NRR parameters were stronger with individualized transverse scaling than with fixed scaling (NRV, slope = 0.005 $mm^3/\mu m$, $R^2 = 0.07$, $P < 0.01$, MRW, slope = 1.72 $\mu m/\mu m$, $R^2 = 0.05$, $P = 0.02$). In addition, these relationships were described as linear because, unlike the relationship of MRW measures and NRV, the ratio of probabilities for AICc analysis did not support the use of an alternative function for the relationship between RNFLV thickness and ONH NRR parameters.

Age-Associated Trends

The RNFL thickness includes neuronal tissue (i.e., the RGC axons) and nonneuronal tissue (i.e., the branches of the central retinal artery and vein and glial tissue), all subject to age-related changes, possibly at different rates.[28,36,41,55,56] The methods of this study allow for analysis of RNFL thickness with and without major retinal vasculature. Based on the results of the effects of scaling on RNFL and ONH parameters, only individually scaled measures were used for the analysis of age-related trends. Both the scaled RNFL thickness, with major

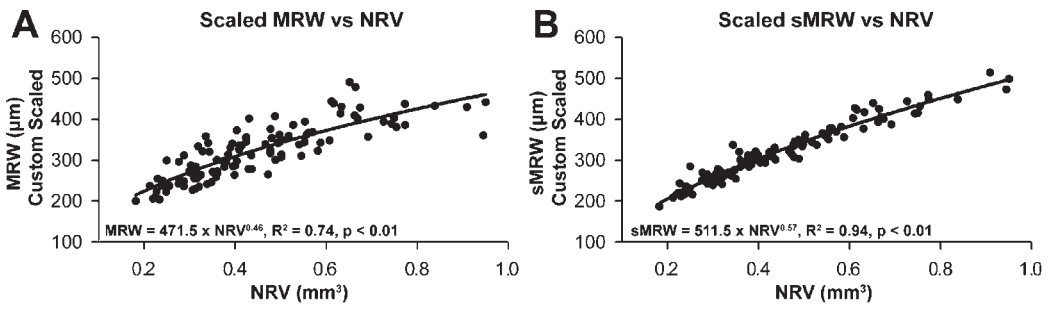

Figure 2. The relationship between the two NRR parameters, MRW and NRV. The relationship between scaled MRW and NRV measures is best described using a simple power function (**A**). The variability is decreased when MRW is scaled to the BMO size (sMRW) as illustrated in (**B**).

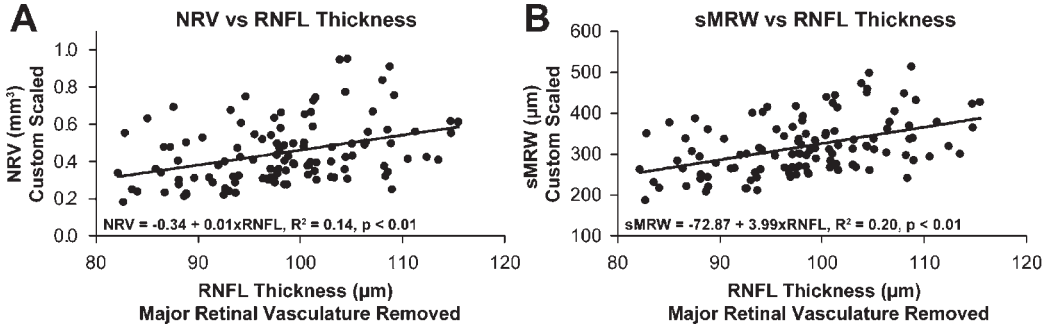

Figure 3. The relationship between NRR measures from ONH analysis and RNFL thickness with major retinal vessels removed. Although there is a significant relationship between these retinal ganglion cell containing structures, there was significant variability for both NRV (**A**) and sMRW (**B**).

retinal vasculature included (Fig. 4A, slope = –0.234 µm/y, R^2 = 0.24, $P < 0.01$) or with the vessels removed (Fig. 4B, slope = –0.206 µm/y, $R^2 = 0.22$, $P < 0.01$) showed significant thinning as a function of age. Although the slopes of the two functions were not significantly different ($F_{1,222} = 0.27$, $P = 0.61$), there was a significant age-related decrease in contribution of the major retinal vasculature to the total RNFL thickness (Fig. 4C, slope = –0.028 µm/y, $R^2 = 0.07$, $P = 0.01$). Consequently, the percentage of thickness from retinal vasculature remained essentially constant across ages (Fig. 4D). These results demonstrate an interesting aging dynamic in the rates of RNFL thinning and reduction of the caliber of blood vessels to maintain a nearly constant proportion of the blood vessels to the total RNFL thickness.

On the face of it, age-related changes in ONH morphology should be confined to structures with RGC axons. This is confirmed by the results of the present study, where the area of the BMO did not show an age dependent change in size (Fig. 5A), while the scaled measures for NRV (Fig. 5B, –0.004 mm³/y, $R^2 = 0.15$, $P < 0.01$), MRW (Fig. 5C, slope = –1.77 µm/y, R^2 = 0.23, $P < 0.01$) and sMRW (Fig. 5D, slope = –1.86 µm/y, R^2 = 0.22, $P < 0.01$) each declined with age. In each case, the aging function was well-defined by linear regression over the range of ages that were assessed. Although sMRW incorporates the size of the BMO, there was no significant difference between the age-dependent slopes for MRW and sMRW ($F_{1,222} = 0.04$, $P = 0.84$).

It is a further expectation that if aging effects in the RNFL and ONH NRR are uniformly related to an age-related loss in RGCs, then the rates of loss should be similar across these anatomically distinct but related areas. The differences in scaled ONH NRR and RNFL rates of change with age were investigated by converting the data to percentages of the mean of the youngest 25 subjects for each measure (Fig. 6). The results demonstrate that the normalized RNFL (data not shown) and RNFLV (Fig. 6, black symbols) thicknesses decreased at a rate of 0.19% and 0.20% per year, respectively, and not statistically different ($F_{1,222} = 0.008$, $P = 0.9$). Similarly, none of the normalized rates of change of neural rim parameters were statistically different with slopes for NRV (Fig. 6, open symbols), MRW (data not shown), and sMRW (gray symbols) of –0.69%, –0.49%, and 0.50% per year, respectively ($F_{2,333} = 0.91$, $P = 0.40$). However, the rates of change with age for ONH NRR parameters were significantly greater than for RNFLV thickness measures ($F_{4,555} = 5.45$, $P <$ 0.01). The differences in rates of change for RNFL and NRR indicate that additional factors are involved in the age-related changes of these retinal structures.

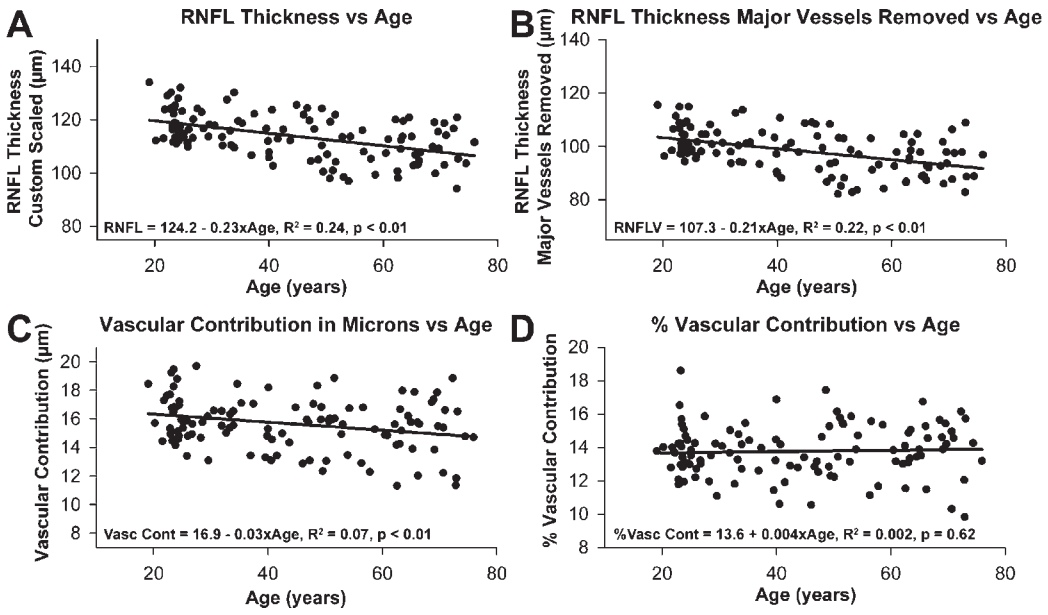

Figure 4. Scaled RNFL thickness with (**A**) and without (**B**) major retinal vasculature decreases with age. When expressed in micrometers, the vascular contribution decreases with age (**C**), but the percent vascular contribution does not change (**D**).

Investigative Ophthalmology & Visual Science

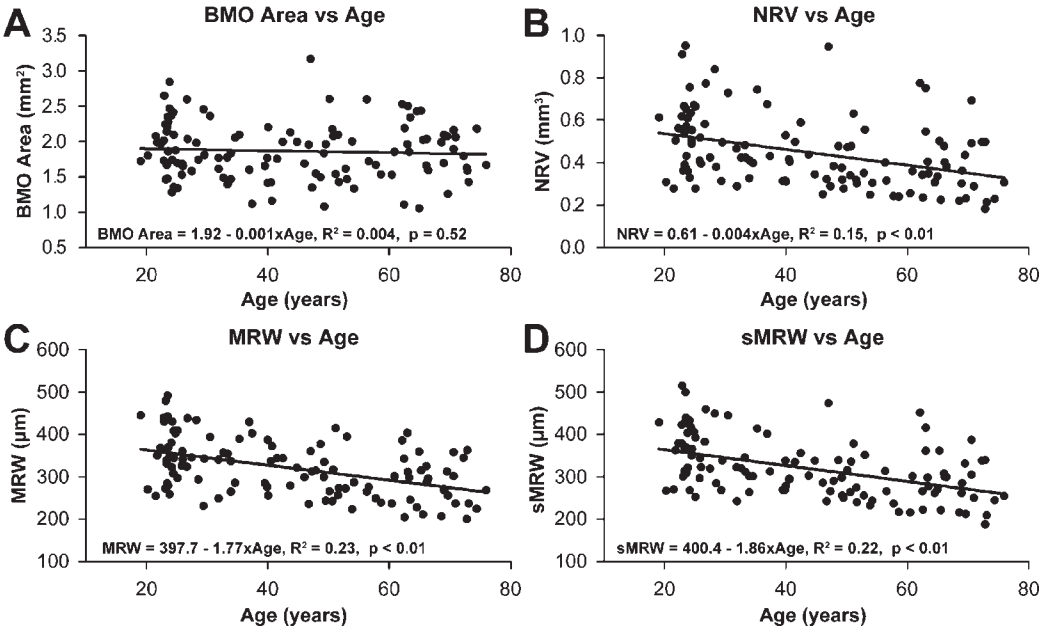

Figure 5. For custom scaled measures, there is no relationship between BMO area and age (**A**). However, NRR parameters of the ONH, including NRV (**B**), MRW (**C**), and sMRW (**D**), all decrease with age. There is no significant difference in the rate of loss for MRW and sMRW, a measure that incorporates the size of the BMO.

Modeling Neural Versus Nonneuronal Changes With Age

The differences in age-related effects on RNFL thickness and ONH NRR parameters provide a purpose for building models of aging, which are based on a foundation that the axonal compositions of the RNFL and ONH NRR are identical and reflect the underlying RGC population and, therefore, differences are likely nonneuronal in nature. The normal aging effect on the RGC population was derived from histological data in six published reports (Fig. 7),[29–33,57] but for comparison to observations of the present study, only data for subjects between 18 and 80 years of age were included. From linear regression on these histological counts, the age-associated loss was estimated at 7209 RGCs/y (Fig. 7, intercept = 1,411,778, $R^2 = 0.18$, $P < 0.01$). Using this linear relationship, the amount of neural contribution at any age to RNFL and ONH NRR measures were estimated (Equation 5) by using an average axon diameter of 0.83, based on an average of previously reported histological measures (0.72, 0.82, and 0.96 µm), assuming that the average axon diameter was uniform in the RNFL and optic nerve and did not change with age.[30,31,57,58] The assumption was also made that the histological techniques used in the literature resulted in only minimal alteration of the axonal diameter.

$$\text{Neural component}(\mu m^2) = (1,411,778 - 7209 \times \text{Age}) \times \pi \times 0.415^2 \quad (5)$$

The neural component for the standard circular scan was estimated by dividing the measure from Equation 5 by the nominal scan circumference of 10,901 µm (Fig. 8A, green line). For the age range of the current study, the slope for predicted RNFL neuronal thickness as a function of age was –0.36 µm/y,

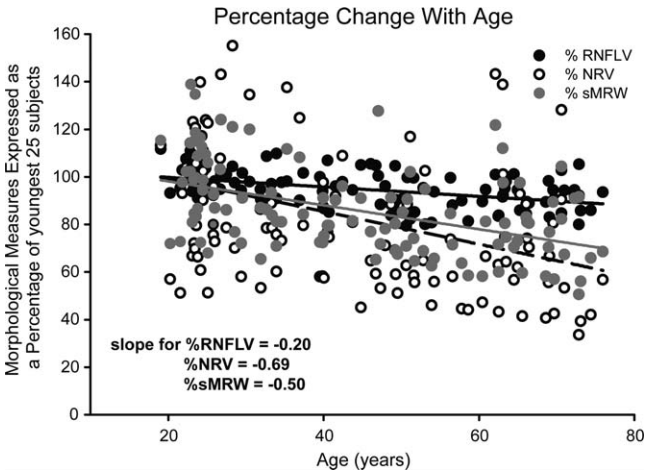

Figure 6. When expressed as a percentage of the youngest 25 subjects, ONH NRR measures show greater change than the circumpapillary RNFL thickness with age.

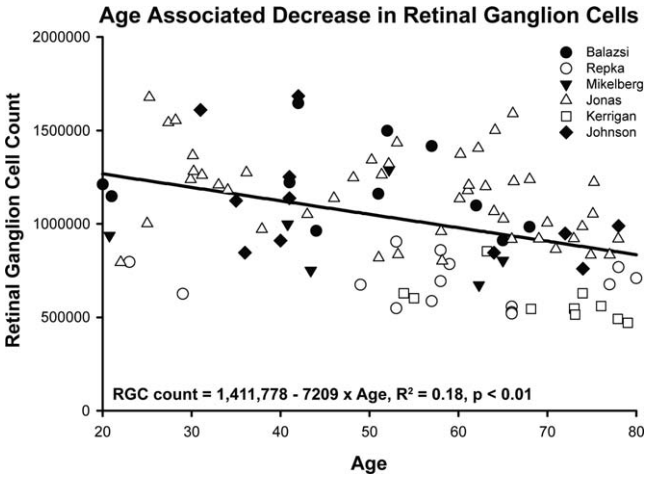

Figure 7. Age-related loss of RGCs estimated from six previously published reports using histological samples.[29–33,57] Only data for individuals between 18 and 80 years of age are shown.

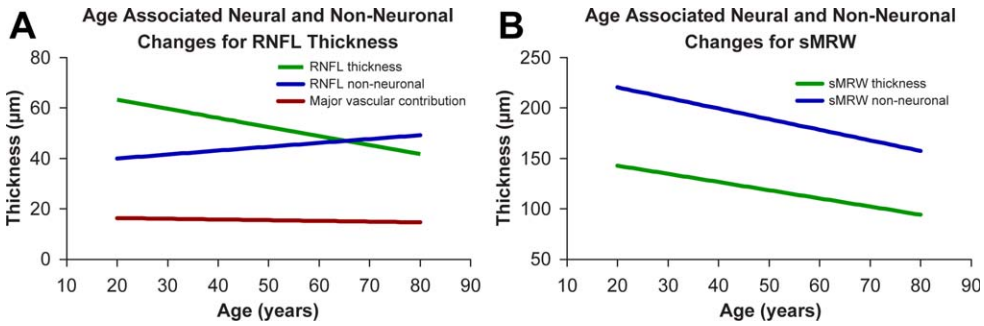

Figure 8. Predicted changes in neural and nonneuronal components within the circumpapillary RNFL (**A**) and MRW (**B**) as a function of age. Whereas an increase in nonneuronal tissue is predicted for the RNFL, the nonneuronal component within the ONH neural rim tissue is expected to decrease with age.

which is significantly different from the measured RNFL slopes, either with (–0.23 µm/y, Fig. 4A) or without (–0.21 µm/y, Fig. 4B) major retinal vasculature ($F_{2,333} = 6.79$, $P < 0.01$). The OCT data were used to calculate the nonneuronal component by subtracting the thickness contribution from the neural component from Equation 5. Based on these calculations, an age-related increase of the nonneuronal component (Fig. 8A, blue line), minus major retinal vasculature (Fig. 8A, red line), of 0.15 µm/y was estimated as the difference between measured thickness, without retinal vasculature, and the predicted RNFL thickness.

For comparison of the neuronal changes in the RNFL with neural changes at the ONH, the sMRW data were similarly modelled. The neural component of the sMRW was estimated by dividing the histological neural component (Equation 5) by the average BMO circumference of 4825 µm. From this calculation, the predicted loss of axons of sMRW was –0.81 µm/y (Fig. 8B, green line) and significantly different from the OCT empirically derived slope of –1.86 µm/y presented in Figure 5D ($F_{1,222} = 10.18$, $P < 0.01$). In contrast to RNFL measures, the nonneuronal component of the ONH NRR tissue is substantial and decreases by –1.05 µm/y in this analysis (Fig. 8B, blue line). Therefore, the models suggest substantially different aging effects of the RNFL and ONH neural rim parameters.

Discussion

In vivo imaging with OCT technology provides high resolution images of the retina and ONH, which provide data for continuing image applications for improvement in the diagnosis and detection in progression of optic neuropathies. For accurate analysis of OCT scans, factors including scan centration,[21,59] scan quality,[19,20,22,60] reference planes,[49] segmentation,[61,62] transverse scaling,[26–28,63] and nonneuronal factors[28,36,41] need to be taken into consideration. The results of the present study demonstrate the agreement between morphological measures of the RNFL, MRW, and NRV and their relationship with age, when individualized transverse scaling is incorporated in well-centered OCT scans.

For accurate and precise morphological measures, several factors, including the location and dimensions of the scan path, need to be taken into consideration and have been studied extensively for the standard RNFL circular scan.[10,53,64–66] For example, a systematic change in both the TSNIT plot and global thickness has been reported with displacement of the RNFL scan path.[21] In addition, RNFL thickness decreases with an increase in distance of the scan path from the ONH rim margin.[64–67] Hence, in longer eyes, in which the scan path is projected further from the rim margin, the RNFL is also thinner.

The effects of ocular magnification on RNFL measures can be corrected, with the assumption that there is minimal change in the RGC axonal content within the circumpapillary region.[68] By incorporating transverse scaling, RNFL thickness can be transformed to an area measure and subsequently to a scaled thickness for a nominal scan circumference.[26,28,53] Although several scaling methods have been proposed, those that include both anterior segment optics and axial length are more accurate.[45] When scaling is applied to RNFL scans, not only is the relationship with axial length not significant, but there is also a reduction in measurement variability as illustrated by the decrease in standard deviation. These scaling methods can also be applied for ONH morphological measures to improve their accuracy and precision.[24,69]

For ONH measures, a significant relationship with axial length was only seen after individualized transverse scaling was applied. Although some studies illustrate a decrease or no change in ONH or BMO size with axial length,[70,71] several investigations, including population-based studies that incorporated scaling, have shown similar results to those presented.[69,72,73] The current results suggest that there is a stretching of the BMO with increase in axial length, with subsequent effects on the ONH neuronal measures. For this study, MRW was scaled to fixed BMO size (sMRW) using similar principles as for RNFL scaling, whereas NRV measures that include the BMO size in their computation were not adjusted for BMO size. Both NRV and sMRW were greater in longer eyes, but this relationship most likely does not represent a larger ganglion cell population in longer eyes, as illustrated by the lack of relationship between BMO area and RNFL thickness. Since there are significant differences in ONH size between ethnic groups,[50,52] these results support studies investigating ethnic differences in ONH morphological measures and including axial length and BMO size when comparing to a normative database.

All three measures, NRV, sMRW, and RNFL, include axons of retinal ganglion cells, and should have good correspondence. Although there was a correlation between scaled RNFL and ONH NRR measures, the significant variability suggests differences in the nonneuronal component that include vasculature and glial tissue. Since the nerve fiber capillary network is continuous and similar to that of the ONH NRR tissue,[74,75] it is not expected that these differences are contributory, at least in healthy normal individuals. However, the variability is most likely a reflectance on glial tissue differences. Specifically, whereas the RNFL has both astroglia and Müller cell processes, the ONH NRR tissue lacks Müller cell processes.[76,77] The differences in nonneuronal tissue may

Investigative Ophthalmology & Visual Science

also explain differences in the relationship of these morphological measures and age.

Age-associated changes in scaled RNFL thickness with and without vasculature removed was similar to those previously published (range ~0.1–0.3 μm/y).[23,34–39] The difference in slopes for the two measures was explained by the age-related decrease in major retinal vascular thickness contribution with age. The thinning of the retinal vasculature (–0.028 μm/y or –0.16 %/y) was similar to the change in retinal vessel diameter reported in the Beaver Dam population (–2.3 μm/y or –0.13%/y).[78] However, the percentage vascular contribution in the present study was similar across ages, indicating a proportional decrease with age-related axonal loss.

Based on previous histological data, the estimated loss of retinal ganglion cells for the age range studied was estimated at 7209 RGCs/y, or 0.36 μm of RNFL thickness per year for an average axon diameter of 0.83 μm.[29–33,57] Using these estimates, the calculated residual RNFL thickness is similar to that reported for eyes with no light perception.[79,80] With the assumption that the axon diameter does not change with age, the model would suggest an increase in nonneuronal tissue with age, similar to that previously modeled using normative data from TD-OCT and standard automated perimetry threshold measures.[36] Since vascular tissue decreases in caliber, the increase in nonneuronal tissue is most likely glial in nature.

For ONH morphological analysis, the MRW is a relatively new optic nerve thickness metric that in principle estimates the RNFL thickness at the BMO.[16,81] And similar to RNFL measures, an age-associated decrease in this measure was noted in the present study (sMRW –1.86 μm/y) that was similar to that previously reported (Chauhan BC, et al. *IOVS* 2014;55: ARVO E-Abstract 4028).[16] Hence, it was ideal to estimate axonal content based on the same principles used for circumpapillary RNFL thickness measures. Based on this analysis, the loss of sMRW would be predicted at 0.81 μm/y with the assumption that all axons were sampled in cross-section.

The differences in age-associated changes of RNFL and ONH NRR parameters are exemplified when measures are expressed as percentages. These findings are in agreement with those from investigators who have investigated normalized age-associated changes in RNFL and ONH parameters using time domain OCT.[82] Specifically, in a study by Sung and colleagues,[82] ONH measures including rim area, cup volume, and vertical integrated rim area changed at a greater rate than RNFL thickness. In addition, when the same assumptions of axon size and RGC loss are used to model sMRW changes, a significant and opposite trend for nonneuronal tissue was noted. The model would suggest that the decrease in nonneuronal tissue is similar in magnitude to that of neuronal tissue. This decrease is likely glial in nature because the vascular changes in this region should be similar to that in the nerve fiber layer; whereas the circumpapillary RNFL contains Müller glia, however, MRW measures do not.

It is also likely that the discrepancy in predicted versus measured MRW relationship with age could represent differences in axonal arrangement with age. For example, in a recent report, Ren and colleagues[43] illustrate an age dependent relationship between anterior lamina cribrosa surface (ALCS) depth and mean deviation. These age related differences in lamina and connective tissue structure could place tension on the axonal fibers subsequently increasing the angular bend at the BMO, compacting the tissue in the region, increasing the axonal density, and consequently decreasing the MRW measured.

In conclusion, RNFL and ONH NRR parameters provide information on the ganglion cell content within the eye that is important for diagnosis and management of optic neuropathy. However, while these measures include the RGC axonal population, there also are significant nonneuronal components and age-related changes that must be considered in clinical application.

Acknowledgments

Supported by Grants K23 EY021761, R01 EY001139, T35 EY007088, P30 EY007551 from the National Institues of Health, National Eye Institute, and the John and Rebecca Moores Professorship (RH), through the University of Houston.

Disclosure: **N.B. Patel**, None; **M. Lim**, None; **A. Gajjar**, None; **K.B. Evans**, None; **R.S. Harwerth**, None

References

1. Quigley HA. Open-angle glaucoma. *N Engl J Med*. 1993;328: 1097–1106.
2. Quigley HA, Miller NR, George T. Clinical evaluation of nerve fiber layer atrophy as an indicator of glaucomatous optic nerve damage. *Arch Ophthalmol*. 1980;98:1564–1571.
3. Sommer A, Katz J, Quigley HA, et al. Clinically detectable nerve fiber atrophy precedes the onset of glaucomatous field loss. *Arch Ophthalmol*. 1991;109:77–83.
4. Weinreb RN, Shakiba S, Sample PA, et al. Association between quantitative nerve fiber layer measurement and visual field loss in glaucoma. *Am J Ophthalmol*. 1995;120:732–738.
5. Quigley HA, Katz J, Derick RJ, Gilbert D, Sommer A. An evaluation of optic disc and nerve fiber layer examinations in monitoring progression of early glaucoma damage. *Ophthalmology*. 1992;99:19–28.
6. Sommer A, Pollack I, Maumenee AE. Optic disc parameters and onset of glaucomatous field loss. II. Static screening criteria. *Arch Ophthalmol*. 1979;97:1449–1454.
7. Teitelbaum BA, Haefs R, Connor D. Interobserver variability in the estimation of the cup/disk ratio among observers of differing educational background. *Optometry*. 2001;72:729–732.
8. Azuara-Blanco A, Katz LJ, Spaeth GL, Vernon SA, Spencer F, Lanzl IM. Clinical agreement among glaucoma experts in the detection of glaucomatous changes of the optic disk using simultaneous stereoscopic photographs. *Am J Ophthalmol*. 2003;136:949–950.
9. Tielsch JM, Katz J, Quigley HA, Miller NR, Sommer A. Intraobserver and interobserver agreement in measurement of optic disc characteristics. *Ophthalmology*. 1988;95:350–356.
10. Schuman JS, Pedut-Kloizman T, Hertzmark E, et al. Reproducibility of nerve fiber layer thickness measurements using optical coherence tomography. *Ophthalmology*. 1996;103: 1889–1898.
11. Blumenthal EZ, Williams JM, Weinreb RN, Girkin CA, Berry CC, Zangwill LM. Reproducibility of nerve fiber layer thickness measurements by use of optical coherence tomography. *Ophthalmology*. 2000;107:2278–2282.
12. Carpineto P, Nubile M, Agnifili L, et al. Reproducibility and repeatability of Cirrus HD-OCT peripapillary retinal nerve fibre layer thickness measurements in young normal subjects. *Ophthalmologica*. 2012;227:139–145.
13. Mwanza JC, Chang RT, Budenz DL, et al. Reproducibility of peripapillary retinal nerve fiber layer thickness and optic nerve head parameters measured with cirrus HD-OCT in glaucomatous eyes. *Invest Ophthalmol Vis Sci*. 2010;51:5724–5730.
14. Wu H, de Boer JF, Chen TC. Reproducibility of retinal nerve fiber layer thickness measurements using spectral domain optical coherence tomography. *J Glaucoma*. 2011;20:470–476.

15. Bussel II, Wollstein G, Schuman JS. OCT for glaucoma diagnosis, screening and detection of glaucoma progression. *Br J Ophthalmol*. 2014;98(Suppl 2):ii15–ii19.
16. Chauhan BC, O'Leary N, Almobarak FA, et al. Enhanced detection of open-angle glaucoma with an anatomically accurate optical coherence tomography-derived neuroretinal rim parameter. *Ophthalmology*. 2013;120:535–543.
17. Mwanza JC, Oakley JD, Budenz DL, Anderson DR; Cirrus Optical Coherence Tomography Normative Database Study Group. Ability of cirrus HD-OCT optic nerve head parameters to discriminate normal from glaucomatous eyes. *Ophthalmology*. 2011;118:241–248.
18. Uchida H, Brigatti L, Caprioli J. Detection of structural damage from glaucoma with confocal laser image analysis. *Invest Ophthalmol Vis Sci*. 1996;37:2393–2401.
19. Savini G, Zanini M, Barboni P. Influence of pupil size and cataract on retinal nerve fiber layer thickness measurements by Stratus OCT. *J Glaucoma*. 2006;15:336–340.
20. Vizzeri G, Bowd C, Medeiros FA, Weinreb RN, Zangwill LM. Effect of signal strength and improper alignment on the variability of stratus optical coherence tomography retinal nerve fiber layer thickness measurements. *Am J Ophthalmol*. 2009;148:249–255.e1.
21. Gabriele ML, Ishikawa H, Wollstein G, et al. Optical coherence tomography scan circle location and mean retinal nerve fiber layer measurement variability. *Invest Ophthalmol Vis Sci*. 2008;49:2315–2321.
22. Sung KR, Wollstein G, Schuman JS, et al. Scan quality effect on glaucoma discrimination by glaucoma imaging devices. *Br J Ophthalmol*. 2009;93:1580–1584.
23. Budenz DL, Anderson DR, Varma R, et al. Determinants of normal retinal nerve fiber layer thickness measured by Stratus OCT. *Ophthalmology*. 2007;114:1046–1052.
24. Savini G, Barboni P, Parisi V, Carbonelli M. The influence of axial length on retinal nerve fibre layer thickness and optic-disc size measurements by spectral-domain OCT. *The Br J Ophthalmol*. 2012;96:57–61.
25. Leung CK, Mohamed S, Leung KS, et al. Retinal nerve fiber layer measurements in myopia: an optical coherence tomography study. *Invest Ophthalmol Vis Sci*. 2006;47:5171–5176.
26. Kang SH, Hong SW, Im SK, Lee SH, Ahn MD. Effect of myopia on the thickness of the retinal nerve fiber layer measured by Cirrus HD optical coherence tomography. *Invest Ophthalmol Vis Sci*. 2010;51:4075–4083.
27. Patel NB, Garcia B, Harwerth RS. Influence of anterior segment power on the scan path and RNFL thickness using SD-OCT. *Invest Ophthalmol Vis Sci*. 2012;53:5788–5798.
28. Patel NB, Wheat JL, Rodriguez A, Tran V, Harwerth RS. Agreement between retinal nerve fiber layer measures from Spectralis and Cirrus spectral domain OCT. *Optom Vis Sci*. 2012;89:E652–E666.
29. Balazsi AG, Rootman J, Drance SM, Schulzer M, Douglas GR. The effect of age on the nerve fiber population of the human optic nerve. *Am J Ophthalmol*. 1984;97:760–766.
30. Repka MX, Quigley HA. The effect of age on normal human optic nerve fiber number and diameter. *Ophthalmology*. 1989;96:26–32.
31. Mikelberg FS, Drance SM, Schulzer M, Yidegiligne HM, Weis MM. The normal human optic nerve. Axon count and axon diameter distribution. *Ophthalmology*. 1989;96:1325–1328.
32. Jonas JB, Schmidt AM, Muller-Bergh JA, Schlotzer-Schrehardt UM, Naumann GO. Human optic nerve fiber count and optic disc size. *Invest Ophthalmol Vis Sci*. 1992;33:2012–2018.
33. Kerrigan-Baumrind LA, Quigley HA, Pease ME, Kerrigan DF, Mitchell RS. Number of ganglion cells in glaucoma eyes compared with threshold visual field tests in the same persons. *Invest Ophthalmol Vis Sci*. 2000;41:741–748.
34. Kanamori A, Escano MF, Eno A, et al. Evaluation of the effect of aging on retinal nerve fiber layer thickness measured by optical coherence tomography. *Ophthalmologica*. 2003;217:273–278.
35. Harwerth RS, Wheat JL. Modeling the effects of aging on retinal ganglion cell density and nerve fiber layer thickness. *Graefes Arch Clin Exp Ophthalmol*. 2008;246:305–314.
36. Harwerth RS, Wheat JL, Rangaswamy NV. Age-related losses of retinal ganglion cells and axons. *Invest Ophthalmol Vis Sci*. 2008;49:4437–4443.
37. Alasil T, Wang K, Keane PA, et al. Analysis of normal retinal nerve fiber layer thickness by age, sex, and race using spectral domain optical coherence tomography. *J Glaucoma*. 2013;22:532–541.
38. Celebi AR, Mirza GE. Age-related change in retinal nerve fiber layer thickness measured with spectral domain optical coherence tomography. *Invest Ophthalmol Vis Sci*. 2013;54:8095–8103.
39. Leung CK, Yu M, Weinreb RN, et al. Retinal nerve fiber layer imaging with spectral-domain optical coherence tomography: a prospective analysis of age-related loss. *Ophthalmology*. 2012;119:731–737.
40. Feuer WJ, Budenz DL, Anderson DR, et al. Topographic differences in the age-related changes in the retinal nerve fiber layer of normal eyes measured by Stratus optical coherence tomography. *J Glaucoma*. 2011;20:133–138.
41. Hood DC, Fortune B, Arthur SN, et al. Blood vessel contributions to retinal nerve fiber layer thickness profiles measured with optical coherence tomography. *J Glaucoma*. 2008;17:519–528.
42. Kotecha A, Izadi S, Jeffery G. Age-related changes in the thickness of the human lamina cribrosa. *Br J Ophthalmol*. 2006;90:1531–1534.
43. Ren R, Yang H, Gardiner SK, et al. Anterior lamina cribrosa surface depth, age, and visual field sensitivity in the Portland Progression Project. *Invest Ophthalmol Vis Sci*. 2014;55:1531–1539.
44. Bennett AG, Rudnicka AR, Edgar DF. Improvements on Littmann's method of determining the size of retinal features by fundus photography. *Graefes Arch Clin Exp Ophthalmol*. 1994;232:361–367.
45. Garway-Heath DF, Rudnicka AR, Lowe T, Foster PJ, Fitzke FW, Hitchings RA. Measurement of optic disc size: equivalence of methods to correct for ocular magnification. *Br J Ophthalmol*. 1998;82:643–649.
46. Bennett AG, Rabbetts RB. The schematic eye. In: Bennett AG, Rabbetts RB, eds. *Clinical Visual Optics*. London: Butterworths; 1989:249–274.
47. Atchison DA, Markwell EL, Kasthurirangan S, Pope JM, Smith G, Swann PG. Age-related changes in optical and biometric characteristics of emmetropic eyes. *J Vis*. 2008;8:29.21–29.20.
48. Bennett AG. A method of determining the equivalent powers of the eye and its crystalline lens without resort to phakometry. *Ophthalmic Physiol Opt*. 1988;8:53–59.
49. Downs JC, Yang H, Girkin C, et al. Three-dimensional histomorphometry of the normal and early glaucomatous monkey optic nerve head: neural canal and subarachnoid space architecture. *Invest Ophthalmol Vis Sci*. 2007;48:3195–3208.
50. Knight OJ, Girkin CA, Budenz DL, Durbin MK, Feuer WJ; Cirrus OCT Normative Database Study Group. Effect of race, age, and axial length on optic nerve head parameters and retinal nerve fiber layer thickness measured by Cirrus HD-OCT. *Arch Ophthalmol*. 2012;130:312–318.
51. Girkin CA, McGwin G Jr, Long C, DeLeon-Ortega J, Graf CM, Everett AW. Subjective and objective optic nerve assessment in African Americans and whites. *Invest Ophthalmol Vis Sci*. 2004;45:2272–2278.

Investigative Ophthalmology & Visual Science

52. Girkin CA, Sample PA, Liebmann JM, et al. African Descent and Glaucoma Evaluation Study (ADAGES): II. Ancestry differences in optic disc, retinal nerve fiber layer, and macular structure in healthy subjects. *Arch Ophthalmol*. 2010;128:541–550.
53. Bayraktar S, Bayraktar Z, Yilmaz OF. Influence of scan radius correction for ocular magnification and relationship between scan radius with retinal nerve fiber layer thickness measured by optical coherence tomography. *J Glaucoma*. 2001;10:163–169.
54. Burnham KP, Anderson DR. Multimodel inference—understanding AIC and BIC in model selection. *Sociol Method Res*. 2004;33:261–304.
55. Ogden TE. Nerve fiber layer of the primate retina: thickness and glial content. *Vision Res*. 1983;23:581–587.
56. Scoles D, Gray DC, Hunter JJ, et al. In-vivo imaging of retinal nerve fiber layer vasculature: imaging histology comparison. *BMC Ophthalmol*. 2009;9:1–9.
57. Johnson BM, Miao M, Sadun AA. Age-related decline of human optic-nerve axon populations. *Age*. 1987;10:5–9.
58. Ogden TE. Nerve fiber layer of the primate retina: morphometric analysis. *Invest Ophthalmol Vis Sci*. 1984;25:19–29.
59. Vizzeri G, Bowd C, Medeiros FA, Weinreb RN, Zangwill LM. Effect of improper scan alignment on retinal nerve fiber layer thickness measurements using Stratus optical coherence tomograph. *J Glaucoma*. 2008;17:341–349.
60. Mwanza JC, Bhorade AM, Sekhon N, et al. Effect of cataract and its removal on signal strength and peripapillary retinal nerve fiber layer optical coherence tomography measurements. *J Glaucoma*. 2011;20:37–43.
61. Asrani S, Essaid L, Alder BD, Santiago-Turla C. Artifacts in spectral-domain optical coherence tomography measurements in glaucoma. *JAMA Ophthalmol*. 2014;132:396–402.
62. Chong GT, Lee RK. Glaucoma versus red disease: imaging and glaucoma diagnosis. *Curr Opin Ophthalmol*. 2012;23:79–88.
63. Sanchez-Cano A, Baraibar B, Pablo LE, Honrubia FM. Magnification characteristics of the Optical Coherence Tomograph STRATUS OCT 3000. *Ophthalmic Physiol Opt*. 2008;28:21–28.
64. Patel NB, Luo X, Wheat JL, Harwerth RS. Retinal nerve fiber layer assessment: area versus thickness measurements from elliptical scans centered on the optic nerve. *Invest Ophthalmol Vis Sci*. 2011;52:2477–2489.
65. Savini G, Zanini M, Carelli V, Sadun AA, Ross-Cisneros FN, Barboni P. Correlation between retinal nerve fibre layer thickness and optic nerve head size: an optical coherence tomography study. *Br J Ophthalmol*. 2005;89:489–492.
66. Savini G, Barboni P, Carbonelli M, Zanini M. The effect of scan diameter on retinal nerve fiber layer thickness measurement using stratus optic coherence tomography. *Arch Ophthalmol*. 2007;125:901–905.
67. Varma R, Skaf M, Barron E. Retinal nerve fiber layer thickness in normal human eyes. *Ophthalmology*. 1996;103:2114–2119.
68. Curcio CA, Allen KA. Topography of ganglion cells in human retina. *J Comp Neurol*. 1990;300:5–25.
69. Leung CK, Cheng AC, Chong KK, et al. Optic disc measurements in myopia with optical coherence tomography and confocal scanning laser ophthalmoscopy. *Invest Ophthalmol Vis Sci*. 2007;48:3178–3183.
70. Nagai-Kusuhara A, Nakamura M, Fujioka M, Tatsumi Y, Negi A. Association of retinal nerve fibre layer thickness measured by confocal scanning laser ophthalmoscopy and optical coherence tomography with disc size and axial length. *Br J Ophthalmol*. 2008;92:186–190.
71. Savini G, Barboni P, Parisi V, Carbonelli M. The influence of axial length on retinal nerve fibre layer thickness and optic-disc size measurements by spectral-domain OCT. *Br J Ophthalmol*. 2011;96:57–61.
72. Oliveira C, Harizman N, Girkin CA, et al. Axial length and optic disc size in normal eyes. *Br J Ophthalmol*. 2007;91:37–39.
73. Ramrattan RS, Wolfs RC, Jonas JB, Hofman A, de Jong PT. Determinants of optic disc characteristics in a general population: The Rotterdam Study. *Ophthalmology*. 1999;106:1588–1596.
74. Hayreh SS. Blood supply of the optic nerve head and its role in optic atrophy, glaucoma, and oedema of the optic disc. *Br J Ophthalmol*. 1969;53:721–748.
75. Hayreh SS. Anatomy and physiology of the optic nerve head. *Trans Am Acad Ophthalmol Otolaryngol*. 1974;78:240–254.
76. Bussow H. The astrocytes in the retina and optic nerve head of mammals: a special glia for the ganglion cell axons. *Cell Tissue Res*. 1980;206:367–378.
77. Ogden TE. Nerve fiber layer astrocytes of the primate retina: morphology, distribution, and density. *Invest Ophthalmol Vis Sci*. 1978;17:499–510.
78. Wong TY, Klein R, Klein BEK, Meuer SM, Hubbard LD. Retinal vessel diameters and their associations with age and blood pressure. *Invest Ophthalmol Vis Sci*. 2003;44:4644–4650.
79. Sihota R, Sony P, Gupta V, Dada T, Singh R. Diagnostic capability of optical coherence tomography in evaluating the degree of glaucomatous retinal nerve fiber damage. *Invest Ophthalmol Vis Sci*. 2006;47:2006–2010.
80. Chan CK, Miller NR. Peripapillary nerve fiber layer thickness measured by optical coherence tomography in patients with no light perception from long-standing nonglaucomatous optic neuropathies. *J Neuroophthalmol*. 2007;27:176–179.
81. Reis AS, O'Leary N, Yang H, et al. Influence of clinically invisible, but optical coherence tomography detected, optic disc margin anatomy on neuroretinal rim evaluation. *Invest Ophthalmol Vis Sci*. 2012;53:1852–1860.
82. Sung KR, Wollstein G, Bilonick RA, et al. Effects of age on optical coherence tomography measurements of healthy retinal nerve fiber layer, macula, and optic nerve head. *Ophthalmology*. 2009;116:1119–1124.

Investigative Ophthalmology & Visual Science